Realcinematographic Visualization of Droplet Ejection in Thermal Ink Jets*

Christian Rembe, Joachim Patzer, Eberhard P. Hofer, and Peter Krehl†

Department of Measurement, Control and Microtechnology, University of Ulm, 89069 Ulm, Germany

†Ernst-Mach-Institut der Fraunhofer Gesellschaft, 79104 Freiburg, Germany

In thermal ink jets a complete understanding of the physical processes in ink-jet firing chambers still requires research. The experimental investigation of these high-speed dynamic processes is difficult due to the extremely short durations of the different phenomena in the ink chamber. For example, the bubble lifetime is approximately 15 μs. A new experimental setup is presented to record phenomena of very short durations, like bubble nucleation, bubble growth, bubble collapse, and the beginning of droplet ejection. This setup allows realcinematographic visualization of such processes with a spatial resolution of less than 1 μm and a time resolution of 10 ns. The apparatus also offers the possibility of studying transient processes such as droplet ejection at high printing frequencies. The essential part of the setup is a new high-speed camera. With an exact evaluation of the digitized images the locus, velocity, and acceleration distributions of the phase interface from liquid to vapor/air can be measured. In addition to experimental work simulation results of a dynamic numerical model with realistic geometric data of the firing chamber and the nozzle of a commercially available printhead are presented. A comparison of experiment and simulation leads to conclusions for pressure propagation in the vapor bubble.

Journal of Imaging Science and Technology 40: 400–404 (1996)

Original manuscript received March 13, 1996.

* Presented in part at IS&T's 11th International Congress on Advances in Non-Impact Printing Technologies, October 29-November 3, 1995, Hilton Head, SC

‡ Current address: Highly Filled Materials Institute at Stevens, Hoboken, NJ 07030, Tel/Fax: (201) 216-5601, E-mail: hgokturk@attila.stevens-tech.edu

Introduction

The successful marketing of thermal ink jets has been facilitated by the integrated semiconductor structure of the device.[1] If printheads are to develop further, it is necessary to understand fully the physical processes in the firing chamber in order to control the ejection of a droplet and to improve resolution and print quality.[2] In this context, one goal is the development of design methods for thermal ink jets. To improve the understanding of bubble jet printers new experimental methods have been developed.

The visualization technology is suited to the measurement of position and velocity. There are two different kinds of visualization methods, *pseudocinematographic* and *realcinematographic* visualization. Pseudocinematographic visualization can be applied to reproducible processes. Such processes are repeated several times and visualized at different points in time. The delay time with respect to the reference point of first shooting corresponds to the interframe time, and this results in a pseudocinematographic sequence of photos. In contrast to that system, the realcinematographic visualization records several frames from a single process realization. This way, nonreproducible (transient) processes can be visualized. Figure 1 shows the principles of the two visualization methods.

So far, processes in thermal ink jets have been studied only by pseudocinematographic visualization. To visualize transient processes, such as the generation of satellite droplets and phenomena at high printing frequencies, realcinematographic visualization must be used. In this study, the two methods are described, compared, and evaluated for visualization of droplet ejection.

Pseudocinematographic Visualization

The following pseudocinematographic measurements have been detected with the experimental setup presented

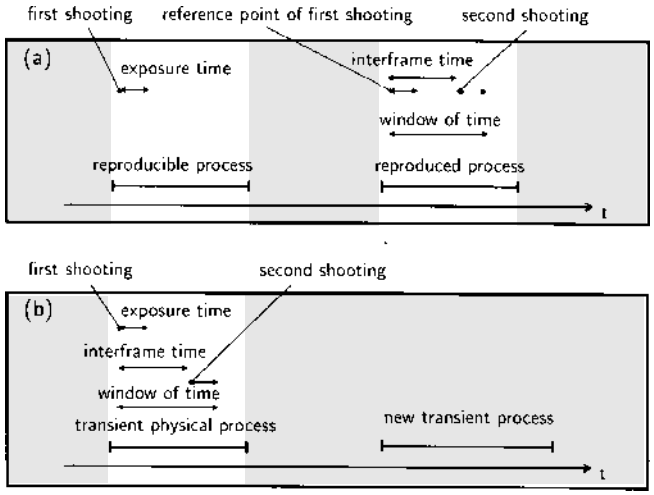

Figure 1. (a) Pseudo- and (b) realcinematographic visualization methods.

by the authors at the IS&T/SPIE symposium in 1994.[2] Figure 2 shows a pseudocinematographic visualization of a droplet ejection of colorless water-based ink.

An objective with a magnifying power of 20 was used, which means the droplet has been imaged with a magnification of 20 onto a CCD array with a pixel size of 11 μm. Thus the pixel resolution amounts to 550 nm. This is less than the resolution of diffraction $g = \frac{\lambda}{\mathrm{NA}}$, with λ the wavelength of light and NA the numerical aperture of the objective. Our light source has peak intensity in the blue-wavelength area (400 to 500 nm), and the objective has a NA of 0.4. As a result, the resolution of diffraction is approximately 1.00 to 1.25 μm for this measurement. Visualizations with an objective having a better numerical aperture have a correspondingly better resolution of diffraction. The best resolution of the setup is at 660 nm with an objective having a NA of 0.75.

The ejection was generated by a heating pulse with a length of 3.3 μs and an amplitude of 13.7 V. With open pool measurements also described in Ref. 2, we have determined that the moment of nucleation is 3.2 μs after firing the heating pulse.

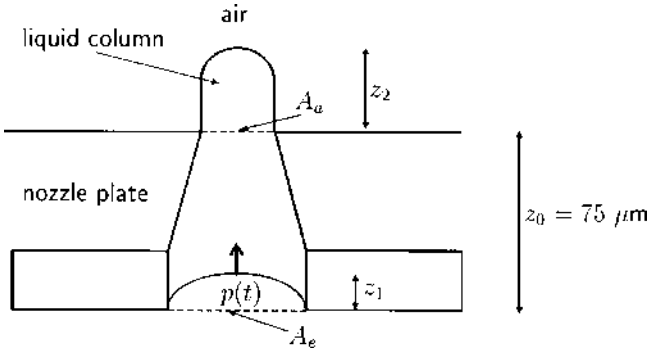

Figure 3. Physical model to determine pressure propagation.

From Fig. 2 it follows that the duration between the moment of nucleation and the first photo with a visible liquid column is 800 ns. The top surfaces of the droplets can be connected by a straight line; consequently, the velocity of the droplet is constant, v = 15.7 m/s. This means that the acceleration occurs at the first 800 ns of droplet ejection after the moment of nucleation. The photo taken 4 μs after firing of the heating pulse shows a liquid column with a height of 4.4 μm. The following section describes how these measured data can be used to determine the pressure propagation in the vapor bubble with a simple physical model.

Evaluation of Cinematographic Photos

To determine the pressure propagation we have assumed that droplet ejection of water-based ink starts as a laminar incompressible flow through a tube. This is shown in Fig. 3. The input plane A_e, in this model the area of the heating element, measures 3600 μm² and the output plane A_a = 2827 μm². We justify the assumption of laminar incompressible flow by the Reynolds number and the number of sound reflections in 1 μs. For the model shown in Fig. 3 the Reynolds number is 450 and this is considerably lower than the critical number of 1160. For values higher than 1160, turbulent flow is possible. The number of sound reflections is 20 in 1 μs, which allows the assumption of incompressibility. In addition, friction and surface tension effects are neglected. The maximum pressure caused by surface tensions can be assessed with the first law of Laplace to

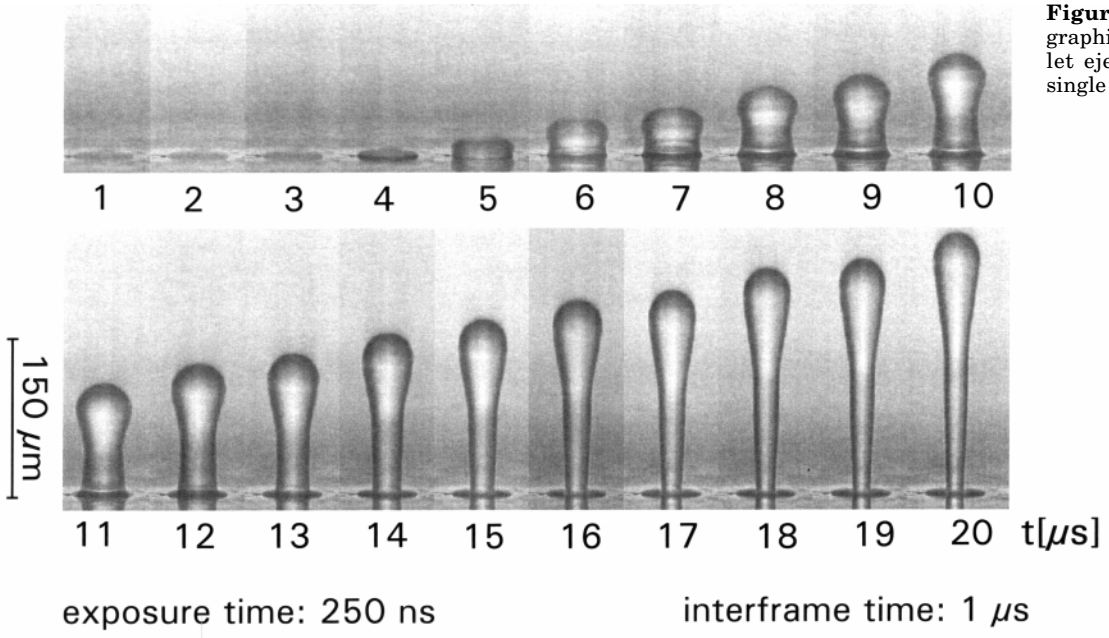

Figure 2. Pseudocinematographic visualization of droplet ejection generated by a single heating pulse.

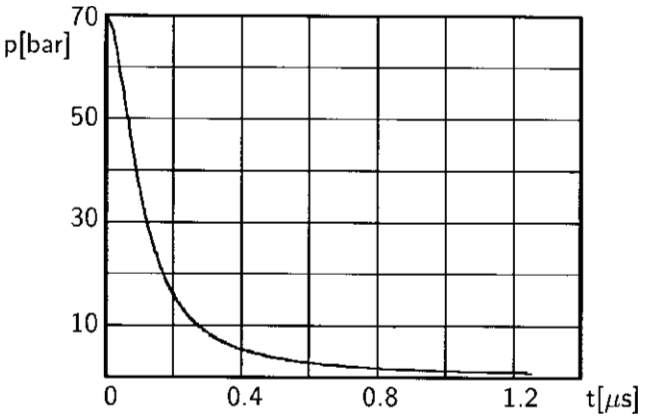

Figure 4. Adiabatic pressure propagation in vapor bubble.

approximately 0.03 bar. The maximum pressure caused by friction can be assessed with the law of Hagen–Poiseuille to approximately 0.04 bar.

To obtain the maximum pressure caused by vapor bubble expansion we have simulated the thermal dispersion[3] of the heating pulse. At the time of nucleation we calculated a temperature of 285.8°C in the lowest layer of liquid. We have used the Antoine equation, which is a modified Clausius–Clapeyron equation, to determine the pressure at the time of nucleation. This pressure has been calculated as p_0 = 69.55 bar. Consequently, the maximum pressure caused by surface tensions and friction is two orders of magnitude smaller than the maximum pressure caused by vapor bubble expansion. With these assumptions the Bernoulli equation,

$$A_1 v_1(t) = A_2 v_2(t), \tag{1}$$

can be used to describe the laminar flow of the liquid. This leads to

$$\dot{v}(t,z) = \frac{A_e}{A(z)} \dot{v}(t,z_1). \tag{2}$$

Accordingly, the dynamics of the process of droplet ejection can be described with the equilibrium between the inertial forces and the force caused by the pressure on the plane of entrance

$$\int_{z_1}^{z_2} A(z)\rho\dot{v}(t,z)dz = (p(t) - p_a)A_e, \tag{3}$$

with p_a the external pressure and ρ the density of the liquid. From Eq. 2 the dynamic equation

$$\left[\left(\frac{A_e}{A_a} - 1\right)z_1(t) + z_0 - h\right]\rho\ddot{z}_1(t) = p(t) = p_a \tag{4}$$

follows, with h the height of the vapor bubble at the beginning of expansion.

The dynamic equation, Eq. 4, can be rewritten as a nonlinear state representation

$$\dot{\mathbf{x}} = \mathbf{f}(\mathbf{x}, u), \tag{5}$$

with $x_1(t) = z_1(t), x_2(t) = \dot{z}_1(t)$, and $u(t) = p(t)$, and the initial conditions $x_1(0) = h$ and $x_2(0) = 0$. Further conditions can be derived from the measured data $x_1(t) = z_1(t_1), x_2(t_1) = \dot{z}_1(t_1)$, and $x_2(t) = x_2(t_1)$ for $t \geq t_1$.

From Fig. 2 it follows that at t_1 = 800 ns the height of the vapor bubble is $x_1 = z_1 = \frac{A_a}{A_e} z_2 = 3.5\,\mu$m and the velocity of the bubble top surface is $x_2 = \dot{z}_1 = \frac{A_a}{A_e}\dot{z}_2 = 12.3$ m/s. At the moment when the pressure in the vapor bubble $p_{crit} = \frac{1}{2}\rho(\dot{z}_2 - \dot{z}_1)^2$, the liquid column starts dragging out and the model is no longer justified. This is the moment when the acceleration of the liquid column stops.

The next step is to find an input function $u(t) = p(t)$ such that the trajectory of droplet ejection passes through the point $\mathbf{x}(t_1)$ in phase space. Note that the number of functions accomplishing this condition is infinite. The pressure propagation is determined by a further very simple assumption. The bubble expansion is assumed to be an adiabatic expansion of an ideal gas with the initial pressure $p(0) = p_0$ = 69.55 bar. The relevant equations read as

$$p(t) = \frac{\lambda}{\left(z_1 A_e\right)^\kappa},\ p(0) = \frac{\lambda}{\left(hA_e\right)^\kappa},\ \kappa = \frac{c_p}{c_v}. \tag{6}$$

This means that one undetermined parameter, h, exists because the parameter λ is defined by $p(0) = \frac{\lambda}{\left(hA_e\right)^\kappa}$. The dynamic equation, Eq. 4, can now be expressed as

$$\dot{z}_1 = \sqrt{2\int_h^{z_1} F(z_1')dz_1'}, \tag{7}$$

with

$$F(z_1) = \ddot{z}_1 = \frac{\lambda - p_a A_e^\kappa z_1^\kappa}{\left(\frac{A_e}{A_a} - 1\right)A_e^\kappa \rho z_1^{\kappa+1} + \rho(z_0 - h)A_e^\kappa z_1^\kappa}.$$

We have evaluated h, using Eq. 7 for $\dot{z}_1$= 12.3 m/s and z_1 = 3.5μm. Consequently, the pressure propagation has been adjusted so that the height of the liquid column is 4.4 μm if the velocity of the droplet front end is 15.7 m/s. The value h has been evaluated as 694 nm, which coincides with the results of the simulation of thermal dispersion. Equation 7 has been solved numerically, using the commercial program MATLAB.

The time dependence of the point $\mathbf{x}(t_1)$ can be used to determine a second parameter (e.g., κ, if polytropic expansion is assumed), or it can be used to verify the assumption of adiabatic expansion of an ideal gas. If the assumption of adiabatic expansion is correct, the trajectory passes through the point $x_1(t_{1,eval})$ = 3.5 μs, $x_2(t_{1,eval})$ = 12.3 m/s at 800 ns with $t_{1,eval}$ the evaluated time for x_1 = 3.5 μm and x_2 = 12.3 m/s. We have calculated $t_{1,eval}$ as 450 ns, which means that the assumption of adiabatic expansion of an ideal gas requires a correction. However, it leads to an estimated error of only 4% for the velocity of the droplet. Figure 4 shows the result of pressure propagation. It is remarkable that the pressure pulse has a width of 150 ns. The pressure propagation reaches p_{crit} at 1.1 μs after time of nucleation.

The pressure propagation shown in Fig. 4 has been used in a numerical model of flow including effects of friction and surface tensions. This model has been presented at IS&T/SPIE 1995 Symposium.[4] Figure 5 shows the simulation results of droplet ejection.

The pressure propagation after 1.1 μs has been adjusted empirically. The velocity of the droplet ejection has been determined as 15.5 m/s. This calculated velocity coincides

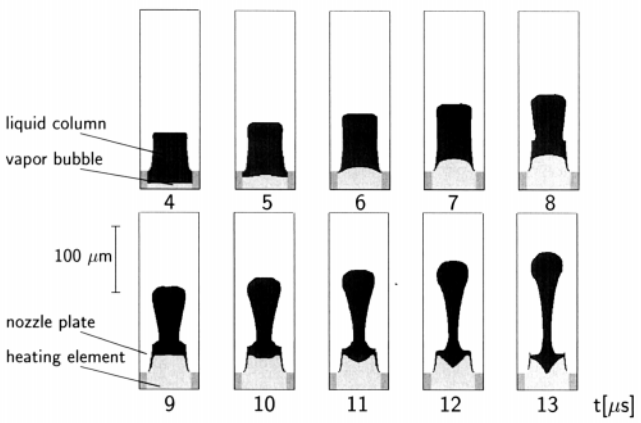

Figure 5. Numerical simulation of droplet ejection.

well with the measured velocity of 15.7 m/s. The pressure propagation illustrated in Fig. 4 is in good agreement with the theoretical investigations of pressure propagations presented in Refs. 5 and 6.

Realcinematographic Visualization

The pseudocinematographic visualization method is not applicable to nonreproducible processes. Figure 6 illustrates the droplet ejection caused by the fifth heating pulse in a burst of heating pulses. The delay between the several heating pulses is 125 μs, which corresponds to a driving frequency of 8000 Hz. Figure 6 clearly indicates that the droplet ejection at 8000 Hz is a transient process for the printhead considered. A trajectory of a droplet cannot be observed. In this case it is necessary to apply a realcinematographic visualization method to observe the trajectories of droplets. Therefore, we have developed a new setup to study high-speed transient processes in micro devices. Although in the case of a thermal ink jet the velocities are not very high for macroscopic proportions (the droplet velocity is ~15 m/s), the necessary magnification of 200 results in a velocity that seems to be 3000 m/s. For the hardware configuration of our setup we have choosen the commercially available high-speed camera IMACON 468 (Hadland Photonics), which we have attached to a microscope. This new setup guarantees the same local resolution as the pseudocinematographic setup. This means that the resolution of the photos is also limited by the resolution of diffraction. The time resolution of the camera is 10 ns. This is the shortest exposure and interframe time.

Another important part of the setup is the light source, which must furnish constant and very intense light for the time window of the observed process. A high intensity of light is necessary to provide short enough exposure time to avoid blur. In addition, highly intense light is required for low gain of the light amplifiers to achieve good signal-to-noise ratio. This aim has been reached by a flashlamp connected to a delay line with different inductive resistors and capacitors. The delay line is designed for furnishing maximum constant current to compensate changing resistance of the flashlamp during the time window. For the droplet ejection application the time window is 100 μs. The intensity of the flashlamp corresponds directly to the current.

The principle of the setup is described as follows: The microscope images the object. The camera, including a beamsplitter composed of eight lenses and a prism, is adjusted to record the image. This adjustment is very sensitive. The beamsplitter parcels the image into eight images, which, at most, can be detected by eight microchannel plate (MCP) sensors. Our setup includes four channels so that we can shoot a maximum of four photos of one transient process.

The exposure times of the channels are defined by the duration of voltage pulses. The interframe times are the distances between the time points of initialization of the voltage pulses. The resolution of exposure and interframe time is 10 ns. The accuracy is much higher and depends on the accuracy of the oscillator crystal in the camera and the rise time of the light amplifiers. The light amplification of an MCP corresponds to the amplitude of voltage applied to the MCP. Consequently, each photo can be referred to its point of shooting, its gain of amplification, and its exposure time. The principle of the camera is illustrated in Fig. 7.

The adjustments of the gains, the interframe times, and the exposure times are dealt with comfortably on a personal computer. The camera has an internal trigger, which makes it possible to set different trigger pulses for the light source or to start the process. It is also possible to control the camera by an external trigger. Figure 8 shows a photo reproduction of a realcinematographic visualization of a droplet ejection generated by a single heating pulse, using our new setup.

The exposure time of this visualization is 600 ns for all photos. Figure 9 shows two realcinematographic visualizations of the 12th droplet of a burst with a 60-μs delay. This corresponds to a printing frequency of 16,667 Hz. For this transient process it is possible to observe the trajectories of droplet ejection marked by asterisks. The two sets of four photos for each of the generated droplets clearly demonstrate the transient nature of this special case. The exposure time of the visualizations is 550 ns for all photos.

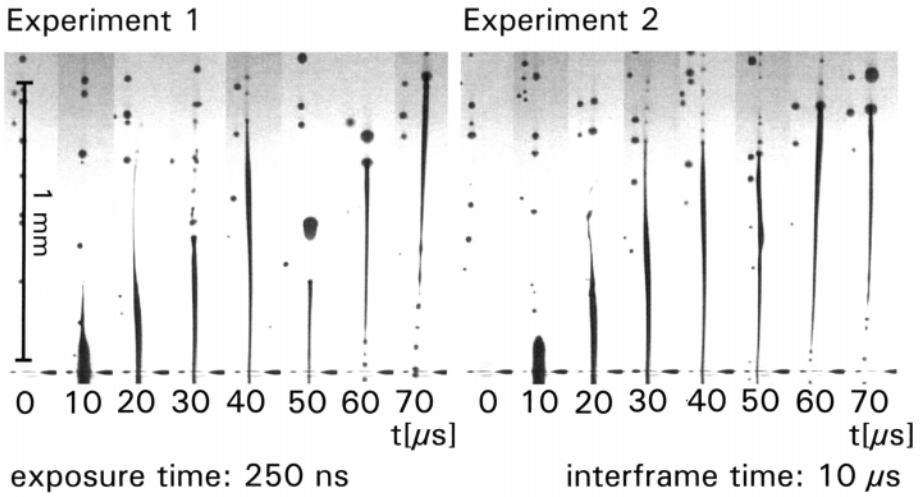

Figure 6. Pseudocinematographic visualizations of droplet ejections generated by a pulse frequency of 8000 Hz.

Conclusions and Outlook

In this study, we first examined the scope and limits of pseudocinematographic visualization. A pseudocinematographic visualization has been successfully incorporated to determine the pressure propagation in a vapor bubble generated by a single heating pulse. The experimental results are in good agreement with our numerical model.

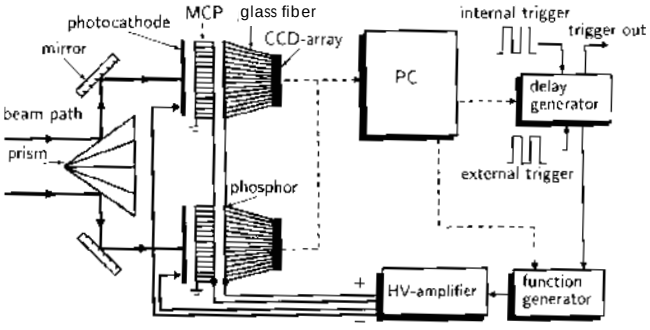

Figure 7. Principle of the high-speed camera.

Then our major concern was to present a new experimental setup for realcinematographic visualization of droplet formation in thermal ink jets. The necessity for this new setup was supported by experiments at high droplet ejection frequencies.

As a final goal, systematic studies of transient processes in thermal ink jets and other micro devices will be carried out. These studies will include the flow in the ink-jet firing chamber, the droplet ejection at very high printing frequencies, and the generation of satellite droplets and their impact on paper.

References

1. E. V. Bhaskar and J. S. Aden, Development of the thin-film structure for ThinkJet® printhead, *Hewlett-Packard J.* **36**: 27 (1985).
2. G. Beurer, E. P. Hofer, and J. Patzer, Process control for improvement of print quality and lifetime of bubble jet printers, *Proc. SPIE* **2171** (1994).
3. J. Patzer, E. P. Hofer, and G. Beurer, Simulation of the influence of different liquids for ink jets under the aspect of color printing, *Proc. SPIE* **2171** (1994).
4. J. Patzer, J. Fuchs, and E. P. Hofer, Surface tension effects in bubble-jet printing, *Proc. SPIE* **2413** (1995).
5. P. A. Torpey, Prevention of an air ingestion in a thermal ink jet device, *Proceedings SPSEs 4th International Congress on Advances in Non-Impact Printing Technol.*, p. 275 (1988).
6. A. Asai, T. Hara, and I. Endo, One-dimensional model of bubble growth and liquid flow in bubble jet printers, *Japan. J. Appl. Phys.* **26**: 1794 (1987).

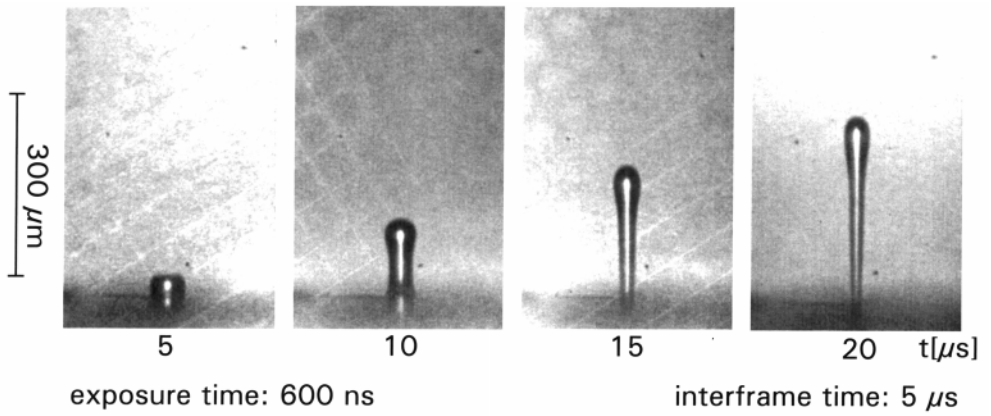

Figure 8. Realcinematographic visualization of droplet ejection generated by a single heating pulse.

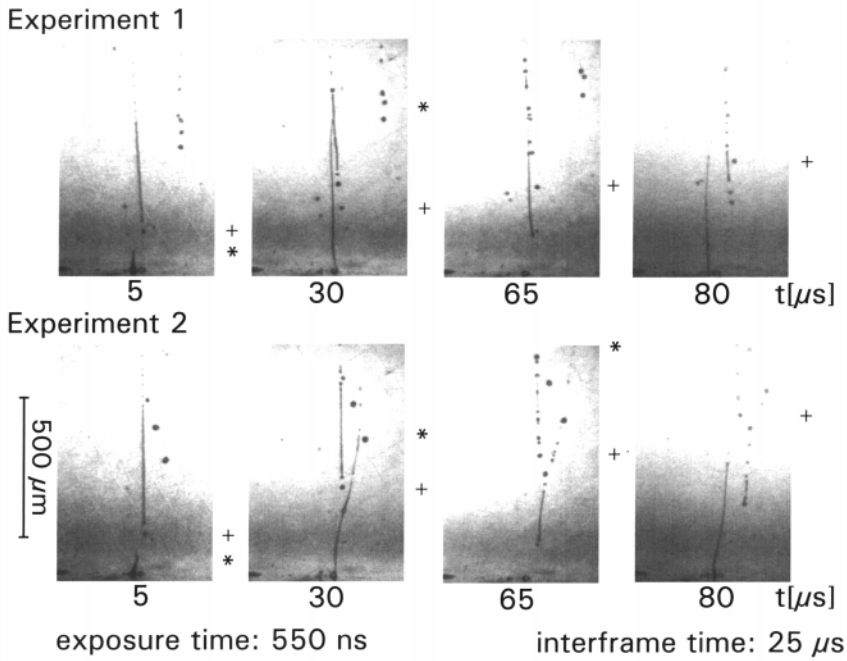

Figure 9. Realcinematographic visualizations of droplet ejections generated by a pulse frequency of 16,667 Hz.